Dynamics of Vesicle Unbinding under Axisymmetric Flow

Sunita Chatkaew,[1] Marc Georgelin,[1] Marc Jaeger,[2] and Marc Leonetti[1,*]

[1]*IRPHE, Aix-Marseille Université, CNRS UMR6594, Centrale Marseille, 13384 Marseille Cedex 13 France*

[2]*M2P2, Aix-Marseille Université, CNRS UMR6181, Centrale Marseille, 13451 Marseille Cedex 13 France*

(Received 4 July 2009; published 8 December 2009)

The competition between adhesion and external flow to unbind settled vesicles from substrates is investigated. An experimental setup is developed to apply a hydrodynamic pulling force in the range of a few piconewtons to a vesicle with retained axisymmetry. In the limit of a small excess of membrane area, vesicles are found to transit during unbinding from a process of fluid film thickening at constant contact area to a finite-time process of contact radius drop to zero with an exponent $1/2$. Both characteristic times vary linearly with the inverse flow rate. On the contrary, deflated vesicles under a moderate pulling force exhibit a decrease of contact area at a constant film thickness before a film thickening.

DOI: 10.1103/PhysRevLett.103.248103 PACS numbers: 87.16.D−, 83.50.−v

The understanding of the dynamics of vesicles [1] under nonequilibrium conditions is receiving increased interest through several approaches: biomimetism applied to active membranes [2], adhesion under pulling force from unbinding [3] to tethers [4,5], and understanding the rheology of biofluids. Indeed, in this last case, recent noteworthy work has furnished new insights—such as a trembling motion (or swinging) for example [6–8]—into the question concerning the effect of shear flow on vesicle shape dynamics in experiments [9–11] as well as in theoretical and numerical investigations [12–15], and broadened significantly the well-known result of Keller and Skalak [16].

If understanding the dynamics of a single vesicle in an unbound fluid is a preliminary essential step, only a few studies have dealt with the interactions between either two (or more) vesicles under flow or fluid constraining walls and vesicle. One notable exception is the theoretical [17] and experimental [18] determination of the 3D lift force which corresponds to the critical force necessary for vesicle detachment under shear flow. Other results are still sparse. This previous physical phenomenon is also reminiscent of vesicle unbinding under a pointlike pulling force, an active research field due to consequences for adhesion between cells, a cell-biological substrate, and more largely, for adhesion between soft substrates (shells here) [3,4,19,20]. In this case also, the critical pulling force (minus its weight) has been determined to be proportional to the equatorial radius R_v (Fig. 1) and to the adhesion energy per unit area W [3] as expected [21]. A power law for the decreasing contact radius R_c (Fig. 1) during unbinding is also predicted with an exponent $1/4$. However, the dynamics of unbinding has not yet been addressed experimentally.

In this Letter, we report the first experimental study of unbinding *dynamics* of a vesicle under an external flow, subject to a wall normal pulling force. To our knowledge, flow has only been used to move a bead stuck to a vesicle [22] and lift-off [18]. Our study is motivated on the one hand by the interaction between wall effects and vesicle dynamics and on the other hand by vesicle unbinding under a pulling force. The necessary critical force is not investigated as this problem has already been studied. In the bulk, a vesicle is characterized by its size $R = (3V/4\pi)^{1/3}$ and its excess area $\Delta = S/R^2 - 4\pi$, S and V are its surface and volume. Various shapes have been identified during unbinding from truncated spheres ($\Delta < 0.1$), egg shape ($\Delta \sim 0.21$) to lipidic tube emergence (deflated vesicles and pointlike force, $\Delta \sim 0.75$). Some shapes are peculiarly reminiscent of recent simulations of vesicle detachment under a pointlike pulling force [19]. Here, we study the unbinding dynamics of an inflated vesicle ($R_c \ll R_v$) and show that it occurs in a two-stage process.

An original experimental setup has been developed to apply hydrodynamic forces, preserving axisymmetry in the

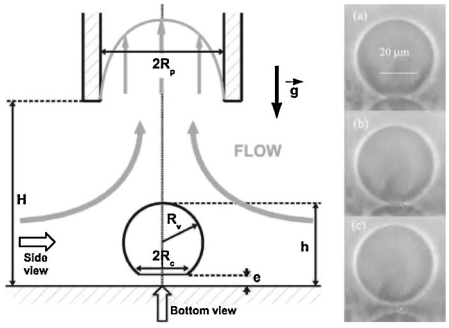

FIG. 1. Schematic setup and example. A settled vesicle is characterized by its radius R_v, its height h and the contact radius R_c. A fluid film of thickness $e \ll R_{c,v}$ between vesicle and substrate results from repulsive disjoining pressure. A large capillary of radius R_p is located above the vesicle to preserve axisymmetry. A suction flow pulls up the vesicle. Visualization is achieved by either the side view or the bottom view (RICM). (a), (b),(c): an inflated vesicle ($R_c \ll R_v$) unbinds.

range 0–50 pN. Indeed, a vesicle on a flat substrate is immobile at the stagnation point of a Stokes flow generated by a suction through a large pipette. The flow pulls the vesicle from the substrate and elongates it along the symmetry axis if the excess area makes this feasible (Fig. 1). If so, the hydrodynamic pulling force becomes time dependent. On the contrary, we expect a constant pulling force on inflated vesicles due to the negligible shape change during all the process. The pulling force has been numerically determined in the same geometry for various radii of a solid sphere (no slip). Comsol software was used. For $H = 100\ \mu$m (Fig. 1), $U = 50\ \mu\mathrm{m\,s^{-1}}$ and $\eta = 1$ mPa s, the range $R_v = 5$–$40\ \mu$m implies a total force of range $F_H = 0.2$–28 pN. Indeed, dimensionally, F_H can be approximated by: $F_H \approx \alpha\eta U \frac{R_v^3}{H^2}$ where $\alpha \approx 48$ (valid for $R_v < 30\ \mu$m).

Two visualizations of vesicles were used: the side view by phase contrast and the bottom view by reflection interference contrast microscopy (RICM [23]). For the bottom view, imaging is obtained by epi-illumination (Hg lamp, filter 546 nm) through a high aperture objective ($\times 60$; NA = 1.4; Oil) mounted on a horizontal microscope (Olympus). RICM visualizes the membrane profile close to the substrate down to 10 nm accuracy. For the side view, the microscope is upright. Thanks to the well design of the bottom of a spectrophotometric chamber ($5 \times 10\ \mathrm{mm^2}$), vesicles are correctly observed by phase contrast (objective $\times 40$; NA = 0.7). All the experiments are done on an *isolated* vesicle transferred gently from a reservoir. A large capillary ($2R_p = 50\ \mu$m) is located precisely above the vesicle at height H (usually, $100\ \mu$m).

Giant vesicles were prepared by electroformation [24]. The lipid solution consisted of 10 mg/mL of EPC (Egg PhosphatidylCholine, Sigma) dissolved in chloroform-methanol (9:1). Here, we only present the results obtained with 200 mM concentration of sucrose whereas the external solution contains glucose (Sigma) from 200 mM to 240 mM. Temperature is maintained at18 °C to minimize convective flows. The adhesion energy per unit area has been evaluated by RICM to the weak value 10^{-8}–$10^{-9}\ \mathrm{J\,m^{-2}}$ [1]. Various vesicles appear inflated, slightly deflated, and deflated with more or less visible thermal fluctuations. The largest ones are chosen to have the best spatial accuracy: $40 \le h \le 60\ \mu$m for phase contrast and $40 \le h \le 95\ \mu$m for RICM visualizations.

Inflated vesicles.—An inflated vesicle characterized by a small contact radius—$R_c \ll R_v$—looks like a truncated sphere. Beyond a critical flow rate U_c, the shape does not change if observed with phase contrast. With slightly deflated vesicles, the vesicle height h increases (pearlike shape) but, it still binds as already observed with a pointlike force [20]. Above U_c, vesicles unbind. It corresponds to a critical pulling force $F_{\mathrm{pull},c}$ which balances buoyancy and adhesion. U_c is unambiguously determined for each vesicle by repeating suctions at different flow rates: close to U_c, the total unbinding time diverges (Fig. 2).

A second report is that during the entire process, before the final detachment, the vesicle height (size) changes less than 1 μm (in the experimental error range), even when R_c decreases. In addition, the contribution of the flow near the wall to the force is small and the excess area conserved, the pulling force remains constant as in the experiments with a pointlike force.

The third report is that the contact radius R_c has the same general variation with time whatever the pulling force (or flow rate U): a plateau (no variation of R_c with time) followed by a finite-time decrease of R_c to zero. During the plateau, the maximum deviation from the resting value is 1 μm: $R_c = R_{c,0} \pm 1\ \mu$m with no continuous decrease at this experimental accuracy. After a time τ_1, the contact radius decreases sharply to zero during a finite time τ_2: see Fig. 2. τ_1 and τ_2 vary with pulling force, vesicle size and contact radius. The curves of Fig. 2 determined by phase contrast do not collapse if time is scaled by $\tau_1 + \tau_2$, the total time of unbinding. As $\tau_1 + \tau_2$ is not the relevant time, a more subtle analysis is necessary, involving two different physical mechanisms during the two stages τ_1 and τ_2.

During τ_1, only RICM provides a new insight as the thickness e of the water film is less than 200 nm $\ll R_{c,v}$ due to the balance between attractive forces (Van der Waals (VdW), buoyancy) and repulsive ones (electrostatic, Helfrich). The water film thickens at the constant contact area (Fig. 3). Quantitatively, RICM measurements show a remarkable exponential growth of the relative film thickness $(e - e_0)$ whatever the pulling force and the initial size of inflated vesicles. The same dynamics appears with slightly deflated vesicles at moderate pulling forces (data not shown) but after a delay. Such a variation can be understood by establishing the balance between viscous dissipation inside the fluid film and the applied pulling force:

$$\eta\pi R_c^2 e\left(\frac{\dot{e}}{e}\right)^2 \simeq (F_{\mathrm{pull}} - F_{\mathrm{pull},c})\dot{e}; \qquad e(t) = e_0 e^{(F_{\mathrm{pull}} - F_{\mathrm{pull},c}/\eta\pi R_c^2)t}. \tag{1}$$

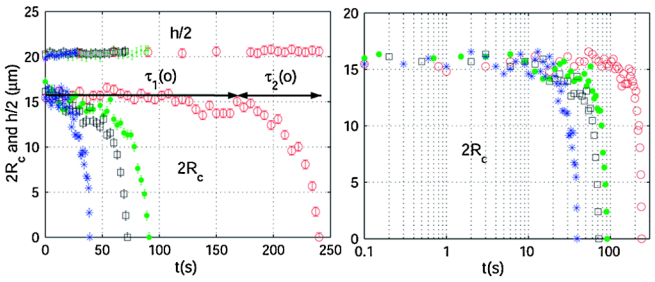

FIG. 2 (color online). Contact diameter $2R_c$ and height h dynamics of one inflated vesicle for decreasing flow rates: $U =$ 37 (○), 38 (●), 39 (□), 43 (*) $\mu\mathrm{m\,s^{-1}}$. Above a critical value U_c (here, $U_c \approx 37\ \mu\mathrm{m\,s^{-1}}$), the vesicle unbinds and its dynamics slows down close to U_c. Two different stages are identified. During a time τ_1, there is no microscopic shape change. During a finite time τ_2, the contact radius decreases to zero while h does not change.

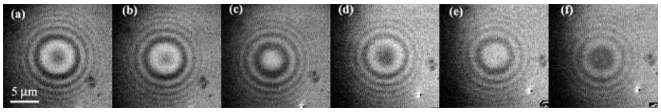

FIG. 3. Contact area of an inflated vesicle during the first stage of duration $\tau_1 = 14.5$ s. The disc at the center corresponds to the contact area observed by RICM: (a) $t = 0$ s, (b) $t = 2$ s, (c) $t = 6$ s, (d) $t = 10$ s, (e) $t = 12$ s and (f) $t = 14$ s. Each interfringe jump corresponds to 100 nm [23]. Here, $2R_v = 110$ μm, $H = 150$ μm and $U = 105$ μm s^{-1}.

After integration, the exponential growth of the thickness (Fig. 4 Left) is effectively recovered. This result can also be found by the Reynolds equation in the relaxation regime: $F_{\text{pull}} < F_{\text{pull},c}$.

Finally, the criterion for defining the two stages is deduced from the following fit: $R_c/R_{c,0} = \Theta(\tau_1 - t) + \Theta(t - \tau_1)[1 - (t - \tau_1)/\tau_2]^n$ where Θ is the Heaviside function and n the characteristic exponent of the finite-time second step of unbinding. Phase contrast measurements (see Fig. 4 Right) show that $1/\tau_1$ is a linear function of the excess of flow rate $U - U_c$, a variation predicted by Eq. (1): $1/\tau_1 = (F_{\text{pull}} - F_{\text{pull},c})/(\eta\pi R_c^2)$. Using force deduced from numerical simulations, $\tau_1 \approx \pi R_c^2 H^2/(\alpha \Delta U R_v^3)$ where $\Delta U = U - U_c$. Indeed, no measurable effect of viscosity on τ_1 was detected using 20% of glycerol in water inside and outside, in the limit of a small excess area. For larger Δ, tip instability and tube emergence are promoted over egg shape. For the cases $U =$ 38–43 μm/s (□) of Fig. 2 for example, τ_1 is approximately a few seconds. For $(R_c, R_v, H) = (8, 20, 100)$ μm, $\Delta U = U - U_c \approx 1$ μm/s, $\tau_1 \approx 5$ s in agreement with experiments.

During τ_2, the physical mechanism is different. Adhesion is overcome. Membrane tension pulls on the contour line of the binding zone to reduce the contact area and lifts off the vesicle. Dynamics results from a balance between viscous dissipation in the region of the corner $\eta\pi R_c^2 e(\dot{R}_c/e)^2$ and the power supplied to the system $-2\pi(\gamma - \gamma_c)R_c\dot{R}_c$ where γ and γ_c are the mechanical tension and its critical value, proportional to the pulling force. Then, the contact radius variation is obtained:

$$R_c(t)/R_{c,0} = (1 - (t - \tau_1)/\tau_2)^{1/2}, \qquad (2)$$

where $1/\tau_2 \propto \gamma - \gamma_c$. Here, for the sake of simplicity, the thickness has been assumed constant as for the deflated vesicles (see further). Consequently, $1/\tau_2$ is a linear function of the excess flow rate, a variation experimentally checked Fig. 5 Right) whatever the inflated vesicle. The finite-time second stage is a power law of exponent $n = 0.47 \pm 0.09$, close to the theoretical value 1/2. This average has been performed on 28 inflated vesicles and for each one on at least 3 flow rates. The exponent value is statistically dominated by the short times.

These results differ from models proposed in the literature [3,25]. In our experimental case, the first stage of the unbinding involves viscous dissipation in the lubrication layer, with no equivalent stage in the models. The adhesion energy is assumed to be constant in the models, whereas the experimental interaction with the substrate varies during the film thickening. During the second stage, the proposed finite-time process involves an exponent 1/4 [3] differing from our 1/2 value. The usual assumption of an evanescent contact angle does not correspond to the experimental situation; however, Fig. 5 shows no marked evolution of the exponent when vesicles with different R_c/R_v, and thus different contact angle, are used. The thickness e of the fluid layer between vesicle and substrate lies in the micrometer range, interestingly close to a value determined by lift-off experiments [18]. As a consequence, this probably weakens the using of the dissipative law of triple line motion. Lastly, the fluid-structure interaction on the large scale of the vesicle does not correspond to the pointlike force of the models. As well, the linear variations of $1/\tau_1$ and $1/\tau_2$ are not explainable by considering two solids submitted to a VdW potential, a pulling force F_{pull}

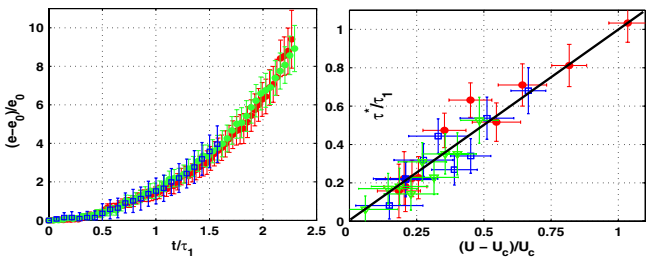

FIG. 4 (color online). Stage 1. Left: Dimensionless thickness dynamics of the liquid film $e - e_0$ between the membrane and the substrate. The time scale is nondimensionalized by $\tau_1 =$ 14 s (●, green [light gray]), 11 s (●, red [medium gray]), 9 s (■, blue) with $2R_c/h = 9/95$ μm respectively ($H = 150$ μm). Right: Linear variation of $1/\tau_1$ with the flow rate determined on three vesicles ($H = 100$ μm): $2R_c/h = 9/38$ μm (●), 11/41 μm (■) μm, 6/32 (▼) μm. τ^* and U_c depend on the vesicle characteristics.

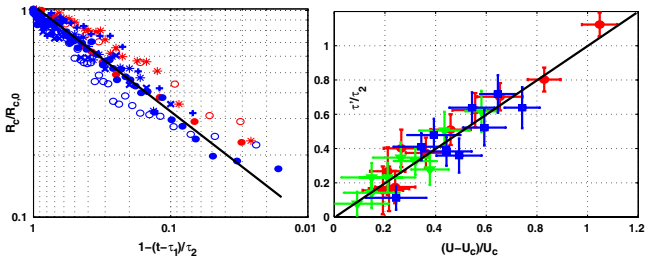

FIG. 5 (color online). Stage 2. Left: Power law of the finite-time process of unbinding. After the time τ_1, contact radius falls to zero in a finite time τ_2: the red (light gray) vesicle (★, $2R_c/h = 12/63$ μm, $U = 72$ μm s^{-1}), (●, $2R_c/h = 15/51$, $U = 38$), (○, $2R_c/h = 11/83$, $U = 170$) and the blue (dark gray) vesicle ($2R_c/h = 14/40$; $U_c \approx 37$) at different flow rates $U = 37$ (○), 38 (●), 45.6 (★), 48.6 (+) μm s^{-1}. The mean value of the exponent is 0.47 ± 0.09 (black line). Right: Linear variation of $1/\tau_2$ with the flow rate. τ' and U_c depend on the vesicle characteristics. See Fig. 4 Right for symbols.

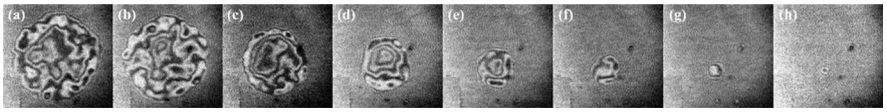

FIG. 6. Unbinding of fluctuating and deflated vesicle. (a) $t = 0$ s, (b) $t = 3$ s, (c) $t = 6$ s, (d) $t = 8$ s, (e) $t = 10$ s, (f) $t = 11$ s, (g) $t = 12$ s, (h) $t = 12.4$ s. Fluctuations are visible during nearly the entire process at constant averaged film thickness: (a) to (g). After, the center color changes successively from deep gray to light gray: (g) to (h). Here, $U = 6\ \mu\mathrm{m\,s^{-1}}$, $H = 25\ \mu$m and $2R_c/h = 38/45\ \mu$m.

and a constant viscous friction between the solids ($1/\tau_{1,2} \propto (U - U_c)^{1/2}$ is expected in this case). Finally, as in the case of lift-off [17,18], the film lubrication plays a central role.

Deflated vesicle at moderate flow rate.—A wide range of dynamics results from the increase of excess area: vesicles elongate, so as to look like truncated eggs. R_c decreases linearly with time. Beyond, a shape singularity appears and a lipid tube results as with pointlike forces [4,5]. By decreasing H to 25–45 μm and the flow rate, hydrodynamic stress is smoothed over a large part of the vesicle. Thus, tip instability is inhibited. During the first stage, as the vesicle elongates strongly along the symmetry axis, the contact radius decreases to zero. The relative fluid film thickness $e - e_0$ remains constant during almost all the detachment (Fig. 6) contrary to inflated vesicles. During the second stage, $e - e_0$ increases quickly compared to the first stage. As $2R_c/h$ has increased (in Fig. 2, $2R_c/h \approx 0.37$ and in Fig. 7, $2R_c'/h' \approx 1.13$), the characteristic time τ_1 from Eq. (2) rises: $\tau_1'/\tau_1 \leq 0.1$ for the same excess force $F - F_c$. Moreover, membrane fluctuations reduce the adhesion energy (e_0 increases): this promotes the beginning of stage 2 compared to the slowing of stage 1. However, with our experimental setup, the pulling force is time dependent making it difficult to go beyond this qualitative picture here ([25] for a track).

To conclude, we have developed an hydrodynamical tool to apply an axisymmetric force (a few pN) to study unbinding dynamics of soft matter. As the thickness is under the optical resolution, RICM was used to complete phase contrast visualization. For inflated vesicles, film thickening at constant contact radius precedes the second stage of decreasing contact radius. In the limit of a small excess area, the approach based on the balance of viscous dissipation corresponds quite satisfactorily to experiments. On the contrary, for deflated vesicles, the contact radius falls to zero at constant thickness before the final rise.

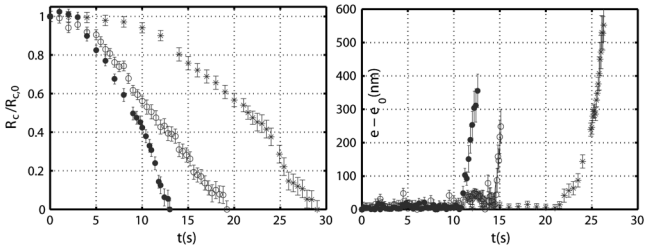

FIG. 7. Unbinding at a constant film thickness. This curve corresponds to Fig. 6 at three different rates. During nearly the entire process, the thickness does not change while the contact radius decreases except at the end where the thickness increases rapidly. Here, $2R_c/h = 45/40\ \mu$m, $H = 45\ \mu$m and $U = 8$ (●), 6.2(○), 4(*) $\mu\mathrm{m\,s^{-1}}$.

We thank J. Deschamps for useful discussions, D. Juric for a critical reading of the text, and A. Viallat for the use of a high aperture objective. This project benefited from a regional PACA grant.

*leonetti@irphe.univ-mrs.fr

[1] U. Seifert, Adv. Phys. **46**, 13 (1997).
[2] P. Girard, J. Prost, and P. Bassereau, Phys. Rev. Lett. **94**, 088102 (2005).
[3] F. Brochard-Wyart and P.-G. de Gennes, C.R. Physique **4**, 281 (2003).
[4] A-S. Smith, E. Sackmann, and U. Seifert, Phys. Rev. Lett. **92**, 208101 (2004).
[5] G. Koster *et al.*, Phys. Rev. Lett. **94**, 068101 (2005).
[6] V. Kantsler and V. Steinberg, Phys. Rev. Lett. **96**, 036001 (2006).
[7] T. Kohyama and G. Gompper, Phys. Rev. Lett. **98**, 198101 (2007).
[8] C. Misbah, Phys. Rev. Lett. **96**, 028104 (2006).
[9] J. Deschamps, V. Kantsler, and V. Steinberg, Phys. Rev. Lett. **102**, 118105 (2009).
[10] V. Kantsler and V. Steinberg, Phys. Rev. Lett. **95**, 258101 (2005).
[11] K. H. de Haas *et al.*, Phys. Rev. E **56**, 7132 (1997).
[12] J. M. Skotheim and T. W. Secomb, Phys. Rev. Lett. **98**, 078301 (2007).
[13] H. Noguchi and G. Gompper, Phys. Rev. Lett. **93**, 258102 (2004).
[14] U. Seifert, Eur. Phys. J. B **8**, 405 (1999).
[15] V. Lebedev, K. Turitsyn, and S. S. Vergeles, New J. Phys. **10**, 043044 (2008).
[16] S. R. Keller and R. Skalak, J. Fluid Mech. **120**, 27 (1982).
[17] U. Seifert, Phys. Rev. Lett. **83**, 876 (1999).
[18] M. Abkarian, C. Lartigue, and A. Viallat, Phys. Rev. Lett. **88**, 068103 (2002).
[19] A.-S. Smith, E. Sackmann, and U. Seifert, Europhys. Lett. **64**, 281 (2003).
[20] A.-S. Smith *et al.*, Biophys. J. **90**, L52 (2006).
[21] J. N. Israelachvili, *Intermolecular and Surface Forces second edition* (Academic Press, London, UK, 1992).
[22] R. Waugh, Biophys. J. **38**, 29 (1982).
[23] J. Rädler and E. Sackmann, J. Phys. II (France) **3**, 727 (1993).
[24] M. I. Angelova *et al.*, Prog. Colloid Polym. Sci. **89**, 127 (1992).
[25] Y. Lin and L. B. Freund, Int. J. Solids Struct. **44**, 1927 (2007).